Supporting Information

Three-layered nanoplates and amorphous/crystalline interface synergism boost CO_2 photoreduction on bismuth-oxychloride nanospheres

Malik Zeeshan Shahid[a], Zhihao Chen[a], Rashid Mehmood[b], Meng Zhang[a], Danrui Pan[a], Shishun Xu[a], Jin Wang[a,c], Ahmed Mahmoud Idris[a,c*], Zhengquan Li[a,c*]

[a]Key Laboratory of the Ministry of Education for Advanced Catalysis Materials, Zhejiang Normal University, Jinhua, Zhejiang 321004, P. R. China

[b]State Key Laboratory of Catalysis, Dalian Institute of Chemical Physics, Chinese Academy of Sciences, Dalian National Laboratory for Clean Energy, Dalian 116023, China

[c]Zhejiang Institute of Photoelectronics, Zhejiang Normal University, Jinhua, Zhejiang 321004, China

Corresponding author

*Email: ahmed503@zjnu.edu.cn; zqli@zjnu.edu.cn

1. Experimental Section

1.1 Chemicals

Ethylene glycol (EG, 99.9 %) and ethanol (99.9 %) were purchased from Xilong Chemical Industry Incorporated Co. Ltd. Poly (sodium 4-styrene sulfonate) (PS, average Mw ~200,000, 30 wt % in H_2O) were obtained from Sigma-Aldrich. Bismuth nitrate pentahydrate ($Bi(NO_3)_3 \cdot 5H_2O$ 99 %) were purchased from Macklin. Sodium chloride (NaCl, NaBr, NaI, 99.9 %), sodium sulfate (Na_2SO_4, 99.9 %), $HAuCl_4$, Na_2PdCl_4, and H_2PtCl_6, were purchased from Sinopharm Chemical Reagents Co. Ltd. Deionized water was prepared with a Milli-Q water purification system. All chemicals were analytical grade and used without further purification. The indium-doped tin oxide (ITO) glass substrates were obtained from China Southern Glass Co., Ltd., Shenzhen. Then they were well cleaned by ultrasonication in a solution containing deionized water, absolute ethanol, and isopropanol for 15 min sequentially.

1.2 Synthesis of BiOCl-NS and other related photocatalysts

For a typical synthesis of BiOCl-NS, 3 mL of 0.25 M $Bi(NO_3)_3$ aqueous solution and 9 mL deionized water were successively injected into 15 mL of EG, in a 50 mL plastic tube under vigorous magnetic stirring. Subsequently, 0.45 mL of PS was added dropwise into the above colourless solution. After stirring for 10 min, 2.5 mL of 3 M NaCl aqueous solution was introduced dropwise and then kept stirring for 30 min till forming a uniform colloid solution. The product was further collected through high rpm centrifugation and was washed repeatedly with water and ethanol. The product was dried at 50 ^oC overnight and stored for characterization and performance study. The final volume ratio of water: EG in the reaction mixture solution is 1:1, and the concentrations of PS, $Bi(NO_3)_3$, and NaCl were 25, 25, and 250 mM, respectively. Further experiments were conducted to expose the influences of reaction time on the formation of BiOCl-NS. Moreover, BiOBr-NS and BiOI-NS were also synthesized by changing the halogen precursor to NaBr and NaI. To synthesize BiOCl-MS, similar conditions (as BiOCl-

NS) were applied except for inserting PS in the reaction vessel. While EG and PS were absent from the system during the synthesis of BiOCl-NP. Furthermore, Au, Pd, or Pt-doped BiOCl-NS were synthesized by using the photo-deposition method (irradiated with Xe light for 30 minutes) with the aid of precursors $HAuCl_4$, Na_2PdCl_4, H_2PtCl_6 respectively.

1.3 Sample characterizations

The products were characterized by transmission electron microscopy (TEM, JEM-1400), field-emission scanning electron microscopy (FESEM, Sigma 500), energy dispersive X-ray spectroscopy (EDS), and high-resolution TEM (HRTEM, JEM-2100F). X-ray diffraction (XRD) was recorded on a Bruker D8 Focus X-ray diffractometer with Cu Kα radiation (λ=0.15418 nm) by depositing the sample on an amorphous silicon substrate. X-ray photoelectron spectroscopy (XPS) was performed on a Thermo ESCALAB 250Xi X-ray photoelectron spectrometer with an Al Kα excitation source, and the binding energies of all elements were calibrated with the C1s peak at 284.8 eV. Nitrogen (N_2) adsorption-desorption isotherms were measured on a Micromeritics TriStar II 3020 instrument at 77 K. Before measurement, the samples were degassed and dried at 200 °C under vacuum for 4 h. The specific surface area was calculated according to the Brunauer-Emmett-Teller (BET) method. The diffuse reflectance spectra (DRS) of BiOCl samples were measured using a UV-Vis-NIR spectrophotometer (Shimadzu UV-3101PC) in the wavelength range of 200 to 600 nm. Photoluminescence (PL) spectra and PL lifetime were recorded on Edinburgh FLS920 Multifunction Steady State and Transient State Fluorescence. Electron paramagnetic resonance (EPR) was measured by Bruker EPR EMXplus. In situ diffuse reflection infrared Fourier transform spectroscopic (in-situ DRIFTS) measurements were conducted using diffuse reflectance infrared Fourier transform spectroscopy (Nicolet iS50, Thermo). The sample was placed in the in-situ reactor equipped with a temperature controller for heating. Firstly, the sample was heated to 100 °C for 2 h to remove the adsorbed water molecules. After being cooled down to room temperature, the background IR spectra were recorded as a reference.

Then CO_2 continuous flow (10 mL/min) was passed through the in-situ pool at room temperature, and after adsorption equilibrium, the sample was irradiated, and IR spectra were recorded simultaneously with a certain time interval.

1.4 Electrochemical procedures

Electrochemical measurements were measured on a Solartron Analytical electrochemical analyzer (ModuLab XM) in a standard three-electrode system by utilizing Pt foil as the counter electrode and Ag/AgCl (KCl, 3 M) as a reference electrode. The working electrodes were prepared by spreading DMF-dispersed slurries of samples (20 mg in a 0.1 mL DMF) onto the well-cleaned ITO glass substrates. Subsequently, the sample-coated substrates were dried in air for 10 min and then annealed at 100 °C for 30 min for electrochemical impedance spectroscopy (EIS) analysis and photocurrent test. In the photoelectrochemical measurements, all three electrodes were placed in a quartz cell containing 0.5 M Na_2SO_4 aqueous solution as the electrolyte which was bubbled by N_2 thoroughly to remove oxygen before the measurement. The transient photocurrent responses were conducted at a bias potential of 0.6 V under a 60 s on/off chopped illumination. The distance between the Xenon lamp and the working electrode was about 2 cm. EIS analysis was measured in the three-electrode system and recorded over a frequency range from 0.01 Hz to 1 MHz with a current voltage amplitude of 0.01 V. Mott-Schtocky measurements were performed at various frequencies 1000 Hz, 1500 Hz, and 2000 Hz.

1.5 Photocatalytic CO_2 reduction

A Pyrex photoreactor was used to execute photocatalytic CO_2 reduction experiments. A simulated light source with a 300 W Xe lamp (Solaredge 700, 100 mW cm^{-2}, 25 °C) was used. The desired photocatalyst (10 mg) was homogeneously dispersed in water (10 ml), and the reactor was evacuated and then purged with CO_2 under continuous stirring several times to remove air completely. Finally, CO_2 gas was filled and the reactor was irradiated at given time intervals. The evolved product (CO) was quantified through periodic headspace gas analysis

(500 μL) using gas chromatography (GC7820A, Agilent). CH_4 was measured using a flame ionization detector (FID), and CO was converted to CH_4 using a methanation reactor and analysed using the FID. To test the reusability of BiOCl-SP, the first cycle (8h) was completed following the procedure described above. For the second cycle, the reactor was evacuated, refilled with CO_2, and run again for 8 h, and the procedure was uninterruptedly performed for four consecutive cycles (approximately 32 h in total).

The selectivity of photocatalytic CO_2 Reduction for CO can be calculated by the following equation:

$$\text{Selectivity (\%)} = R_{CO}\times 2 / (R_{H2}\times 2 + R_{CO}\times 2 + R_{CH4}\times 8) \times 100\%$$

Where R_{H2}, R_{CO} and R_{CH4} are the production rates of photocatalytic reactions of H_2, CO and CH_4.

The corresponding apparent quantum yield (AQY) of the BiOCl-NS for the product generation was calculated through the following equation:

$$AQY = \frac{N_e}{N_p} \times 100\%$$

$$N_e = [2 \times (n_{H2} + n_{CO}) + 8 \times n_{CH4}) \times N_A$$

$$N_p = \frac{IAt\lambda}{hc}$$

Where N_e is the total number of reactive transfer electrons, and N_p is the number of incident photons. where n_{H2}, n_{CO} and n_{CH4} is the H_2, CO and CH_4 production amount (15, 8 and 85 μmol) per hour under different band-pass filters, N_A is the Avogadro constant (6.02×10^{23} mol^{-1}), h is the Plank constant (6.626×10^{-34} J s^{-1}), c is vacuum light velocity (3×10^8 m s^{-1}), λ is the monochromatic light wavelength (420 nm), t is the light irradiation time (1 h = 3600 s), I is the incident monochromatic light intensity (30 W/m^2), A is the irradiation area (5.7 cm^2).

The turnover number (TON) of BiOCl-NS was estimated from the following formula;

TON= (Number of moles of CO evolution)/(Number of moles of BiOCl-NS taken)

1.6 DFT simulations

All DFT calculations in this work were performed by the Vienna Ab-initio Simulation Package (VASP). The electron-ion interaction was described by the projector augmented wave (PAW) pseudopotential method, and exchange-correlation energy was described by Perdew-Burke-Ernzerhof (PBE) in generalized gradient approximation (GGA). The Monkhorst-Pack grid mesh-based Brillouin zone k-points are set as 2×2×1 for all surface structures with the cutoff energy of 450 eV and the equilibrium was reached when the forces on the relaxed atoms became less than 0.05 eV/Å. Furthermore, the (110) facet was selected as a typical catalysis active surface of BiOCl. To avoid interlayer interference, a 20 Å vacuum layer along the Z direction is employed.

2. Supplementary Figs. (S1-S20)

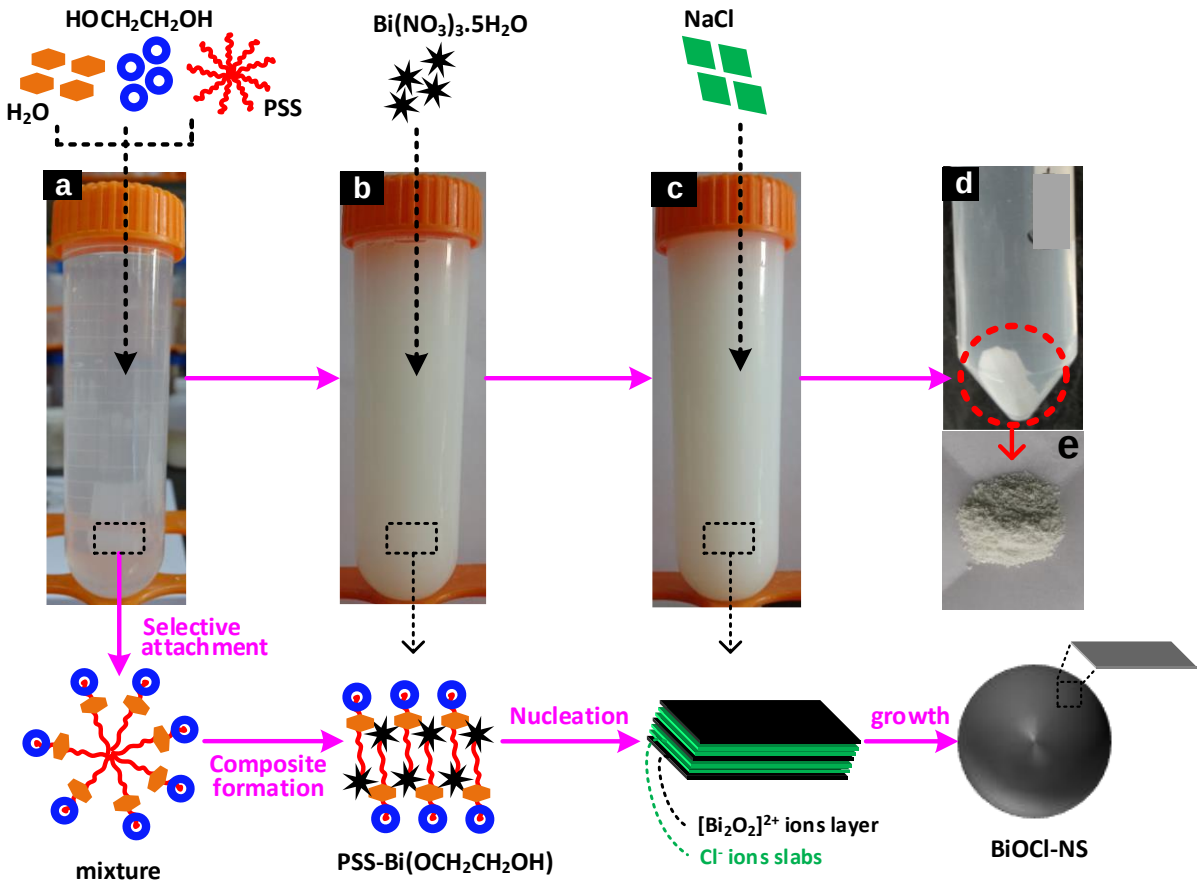

Fig. S1 The formation process of BiOCl-NS with real-time photographs, displaying the synthesis propagation with typical complex generation after the addition of EG, Water, PS, and Bi precursor.

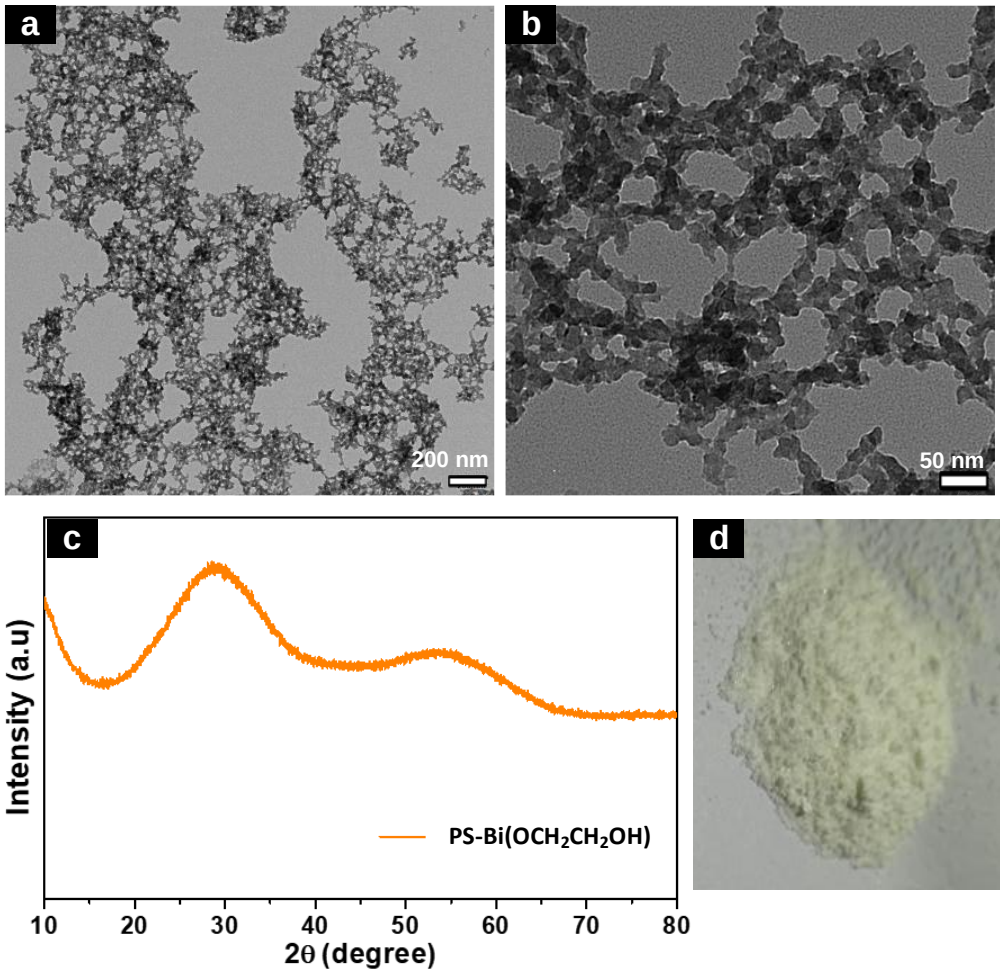

Fig. S2 (a, b) TEM images of complex (PS-Bi(OCH_2CH_2OH) formed during the synthesis of BiOCl-NS at RT. (c) Corresponding powder and XRD pattern of composite.

The temporary composite thus restricts the sudden contact between bismuth precursors and halogen precursors. This leads to the controlled, non-agglomerated formation of 3D-structured BiOCl-NS.

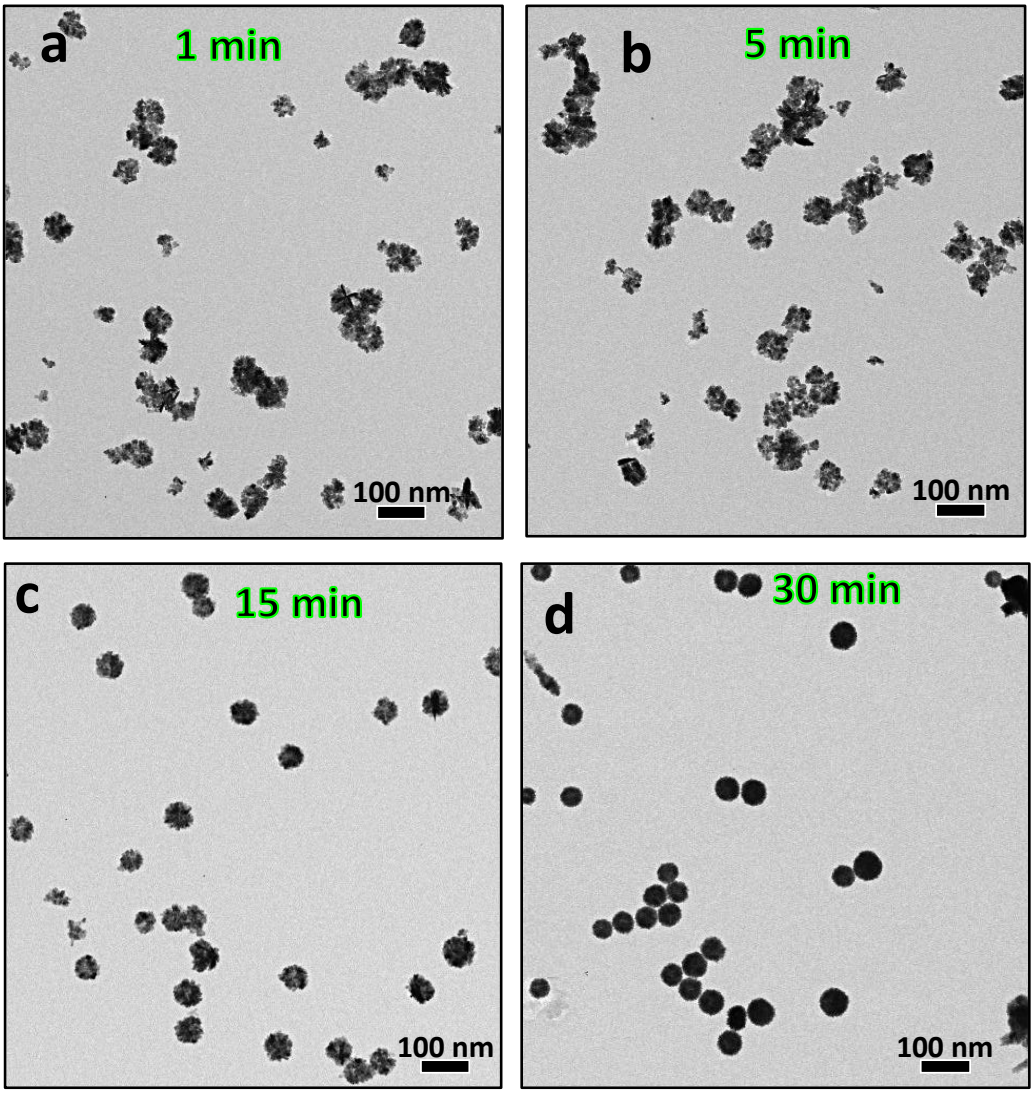

Fig. S3 (a-d) Time-dependent structure evolution of BiOCl-NS.

The structural transition from the relatively open morphology to regularly-confined morphology. That confirms that innovatively controlling the synthesis route, can inhibit the conventional habitual growth to micron size.

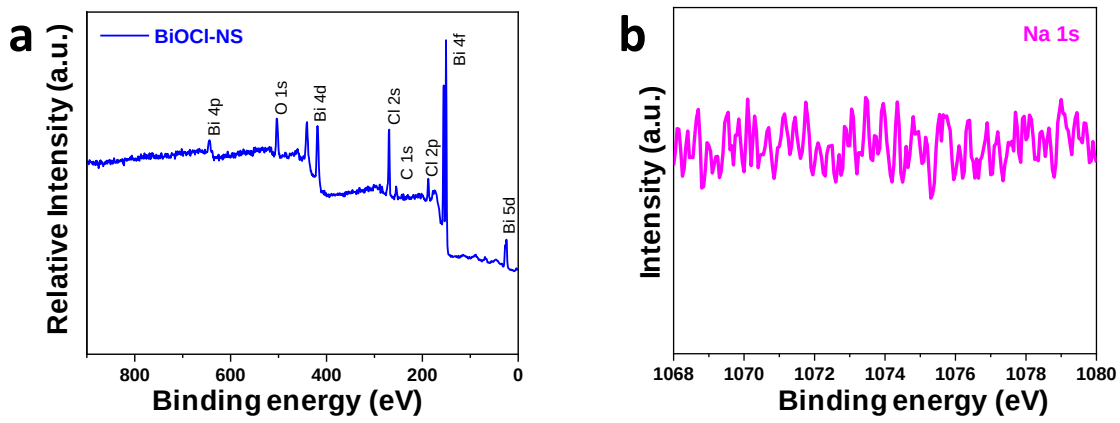

Fig. S4 (a) XPS survey spectrum, (b) high-resolution XPS spectra of element Na 1s, ruling out the existence of PS residues on the surface of BiOCl-NS.

The absence of any Na1s signal further validates that PS has just participated temporarily during the formation process, and it has not been detected in BiOCl-NS, confirming the purity of the product.

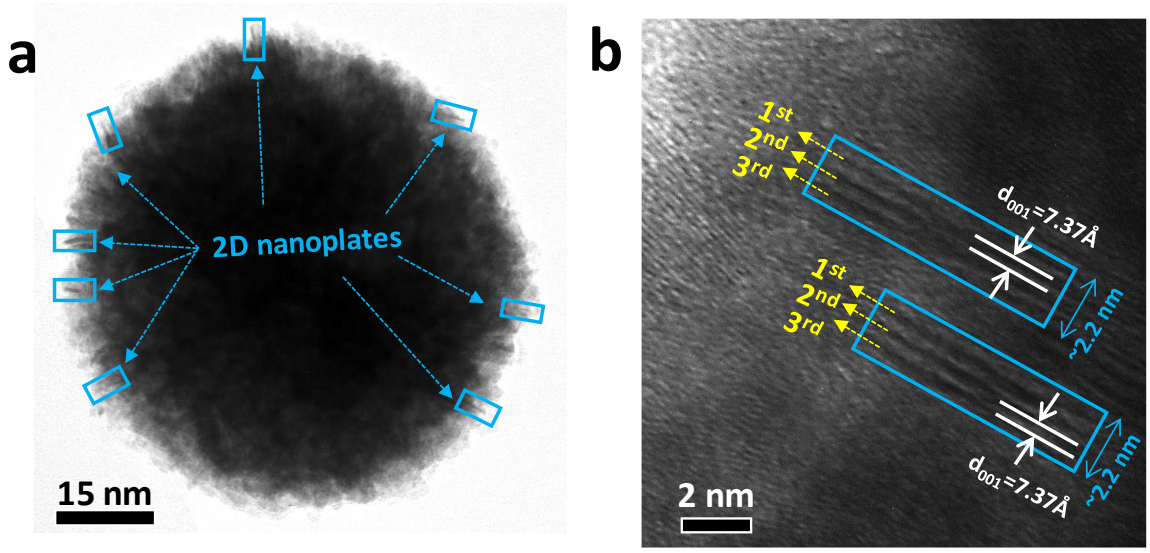

Fig. S5 HRTEM images of BiOCl-NS (a) single nanoparticle, (b) three-layered nanoplates configuration.

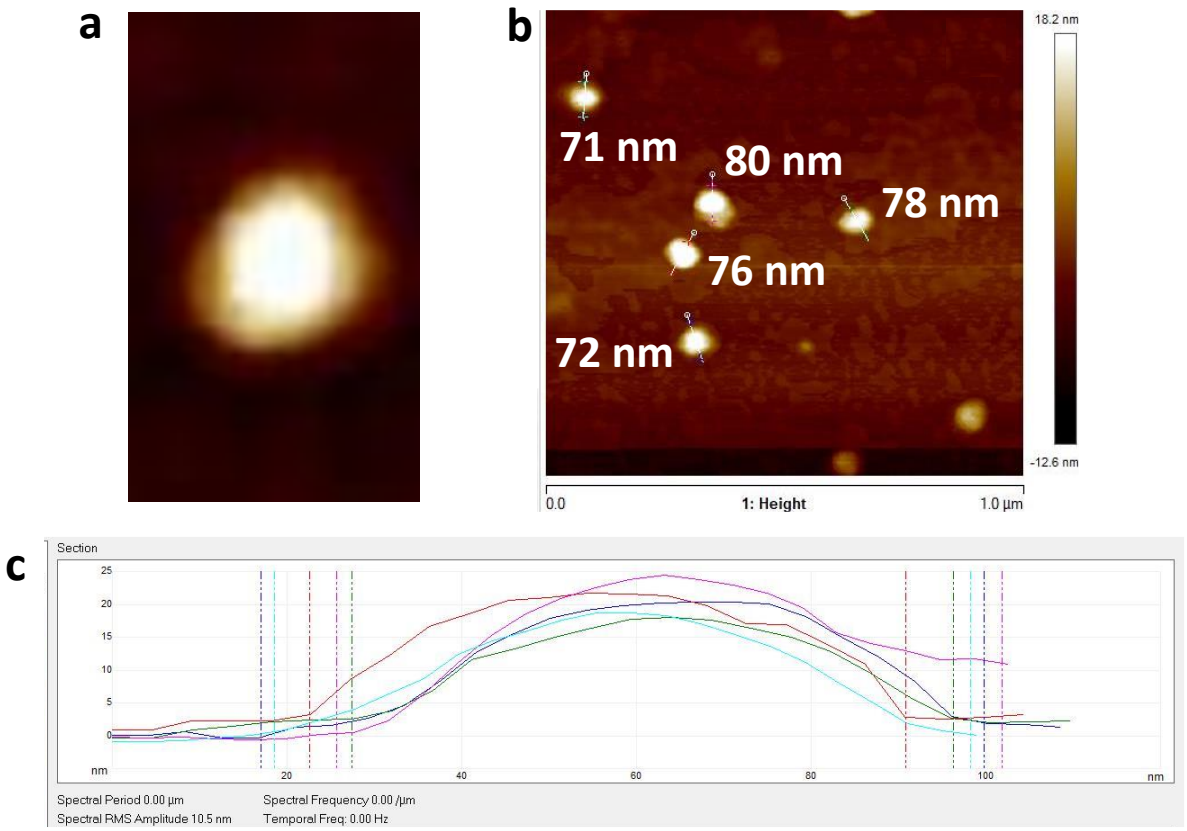

Fig. S6 (a, b) AFM images and (c) corresponding height profile.

AFM image of a single particle of BiOCl-NS showing a distinct morphology, and size distribution of various nanoparticles. The profile is based on the individual particles' distance from one point to another, further confirming the diameter distribution of BiOCl-NS.

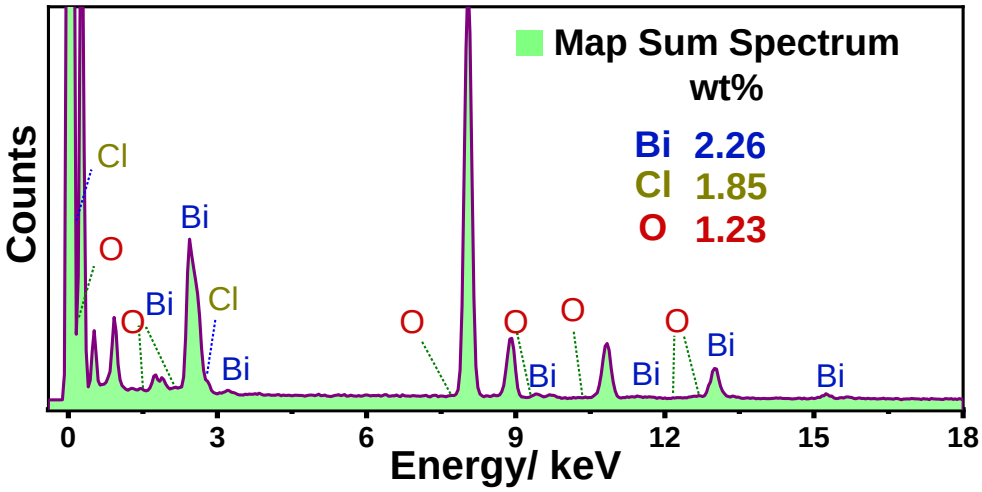

Fig. S7 EDS spectra highlight a relatively lower weight percentage of element O in BiOCl-NS.

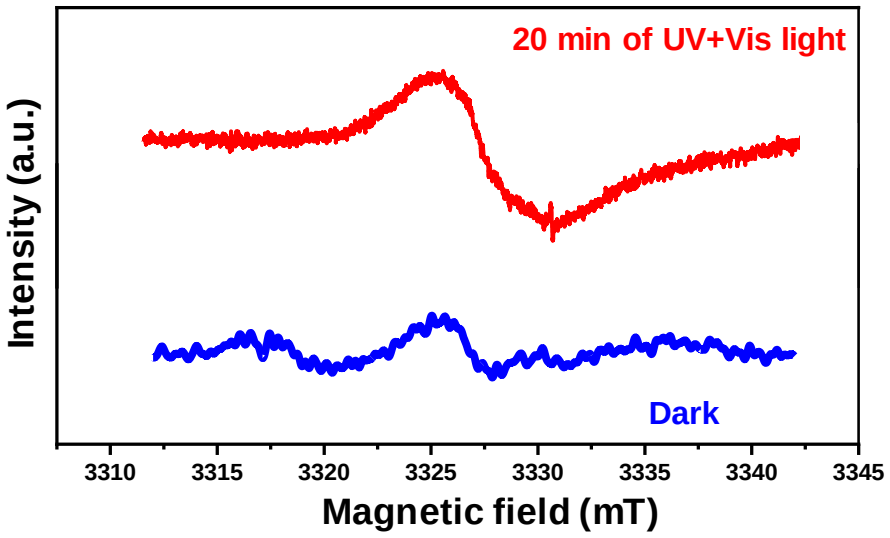

Fig. S8 EPR spectra of BiOCl-NS after 10 min of light irradiation in comparison to dark conditions, demonstrating the existence of dynamic or light-induced defects.

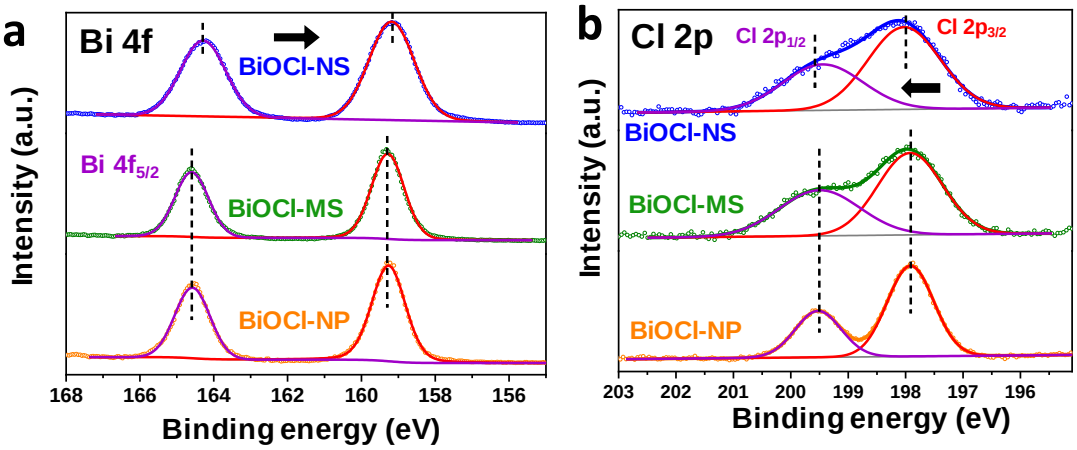

Fig. S9 Comparative illustration of high-resolution *ex-situ* XPS spectra of (a) Bi 4f and (b) Cl 2p.

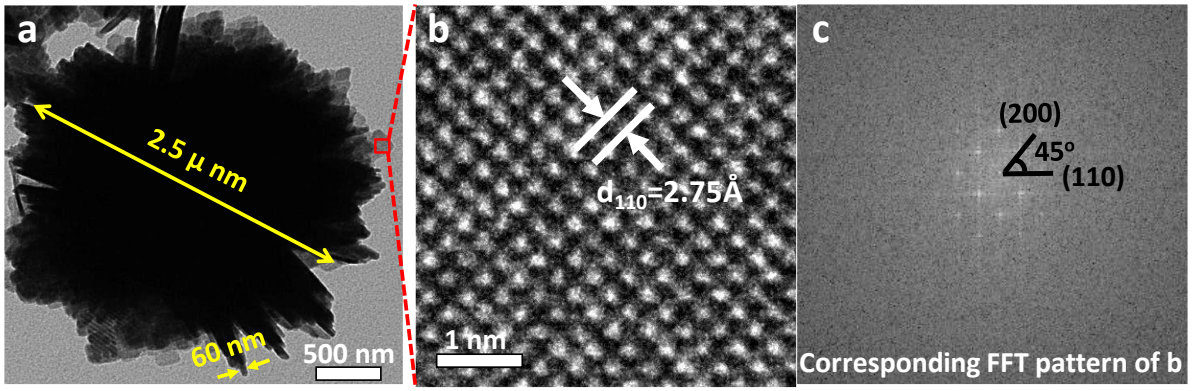

Fig. S10 (a) TEM image of BiOCl-MS displaying about ~2.5 um diameter and thickness of about ~60 nm. (b) Lattice distribution and (c) corresponding FFT pattern.

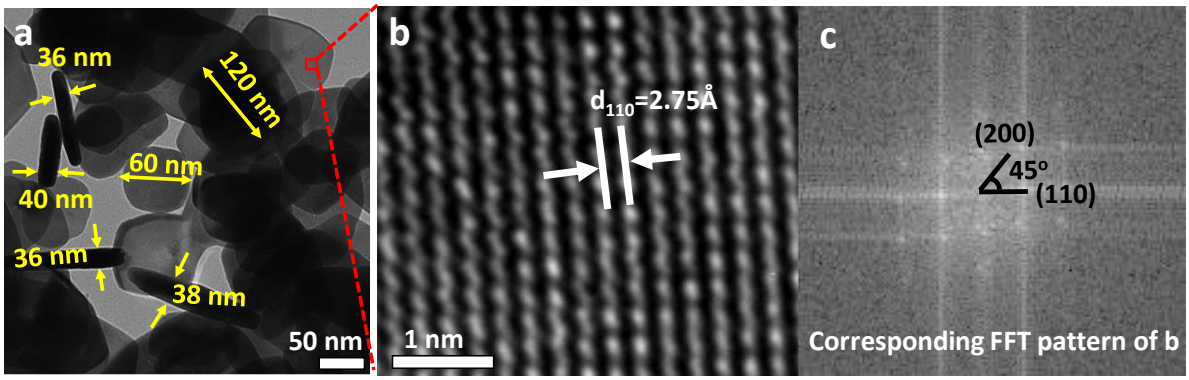

Fig. S11 (a) TEM image of BiOCl-NP demonstrating nanoplates randomly distributed horizontally and vertically with planar size range from 60-120 nm, and thickness ranging from 36-40 nm. (b) Lattice distribution and (c) corresponding FFT pattern.

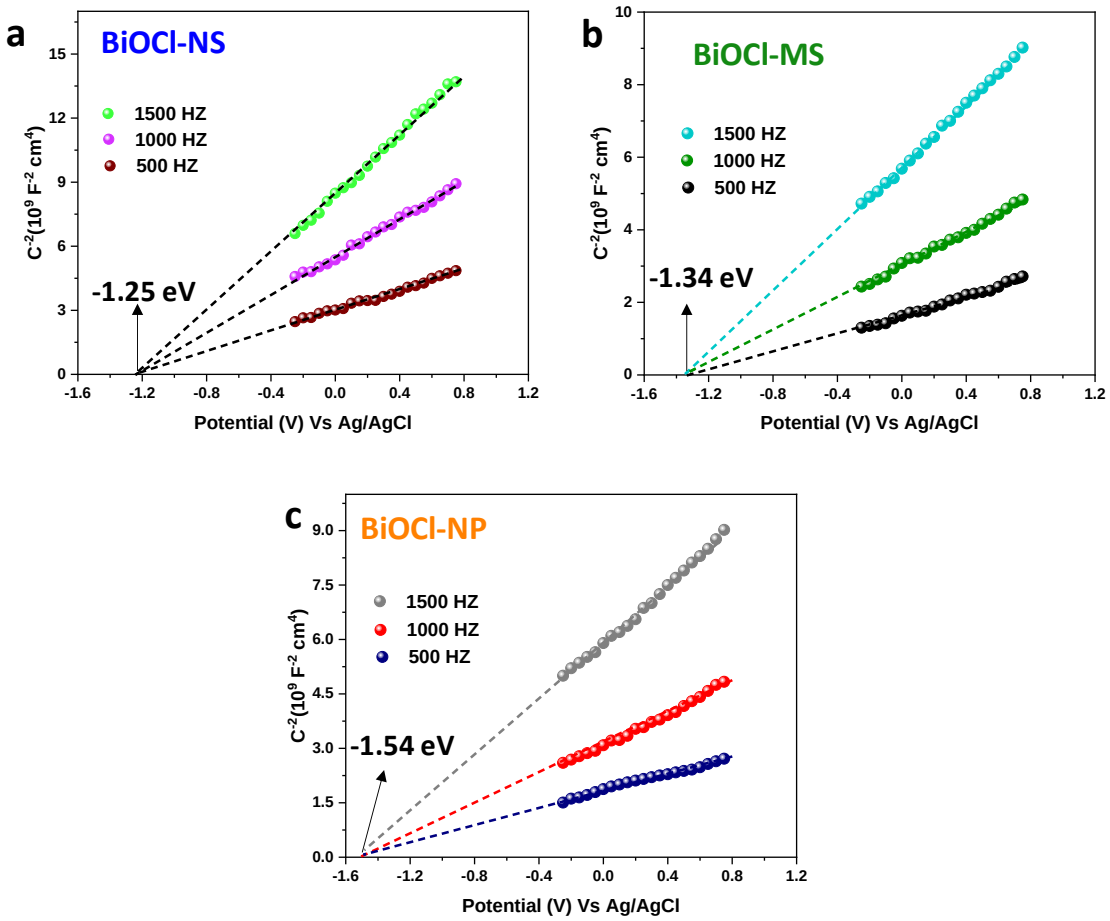

Fig. S12 Mott Schottky analysis of (a) BiOCl-NS, (b) BiOCl-MS, and (c) BiOCl-NP measured at different frequencies. (d) Band alignment showing corresponding CB and VB positions of BiOCl-NS, BiOCl-MS, and BiOCl-NP.

The flat band (E_{FB}) for BiOCl-NS, BiOCl-MS and BiOCl-NP was found to be -1.25 V, -1.34 V, and -1.54 V against Ag/AgCl. As is known, BiOCl is an indirect semiconductor whose flat band is very close to VB, considering this, E_{CB} was calculated against NHE using the following formula [$E_{NHE} = E_{Ag/AgCl} + E^{o}_{Ag/AgCl} + 0.059.\ pH$]. Where, the value of $E_{Ag/AgCl}$ is -1.251 V for BiOCl-NS and -1.34 V for BiOCl-MS, and -1.54 V for BiOCl-NP, $E^{o}_{Ag/AgCl}$ = 0.199 V, and pH= 7. Accordingly, the E_{CB} values were calculated to be -0.63 V, -0.72 V, and -0.92 Vs NHE for BiOCl-NP, BiOCl-MS and BiOCl-NS, respectively. Further, by using the equation $E_{VB} = E_g - E_{CB}$, the values of the valence band potential (E_{VB}) turned out to be 2.74 V, 2.54 V, and 2.02 V for BiOCl-NP, BiOCl-MS and BiOCl-NS, respectively.

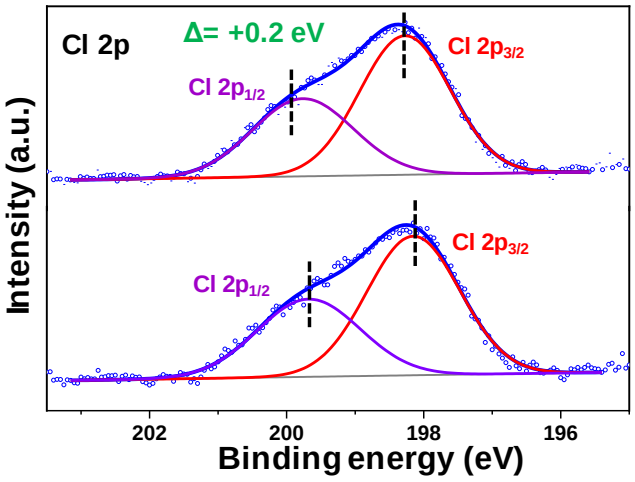

Fig. S13 *In-situ* XPS spectra of Cl 2p under simulated light irradiation in comparison to the dark conditions.

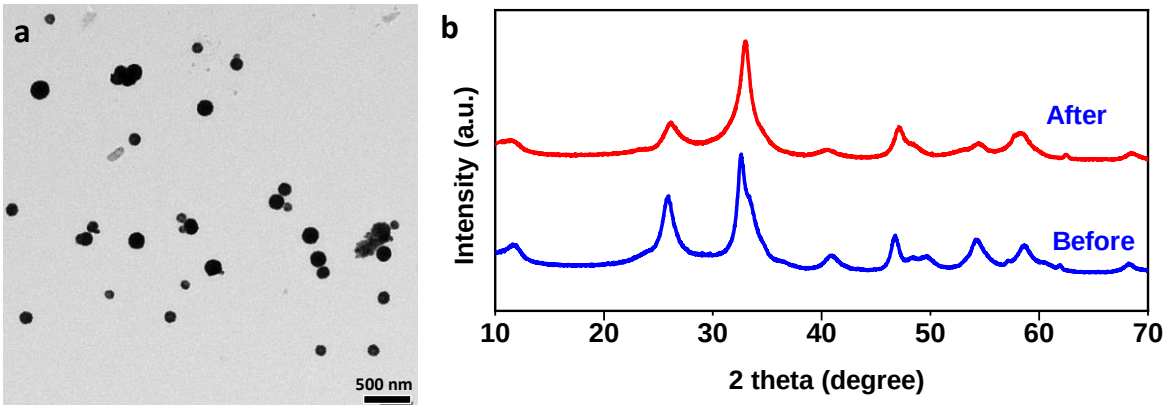

Fig. S14 The characteristics of BiOCl-NS after reusability, (a) TEM and (b) XRD pattern.

The results confirm the morphological and phase purity after using BiOCl-NS for consecutive photocatalytic cycles.

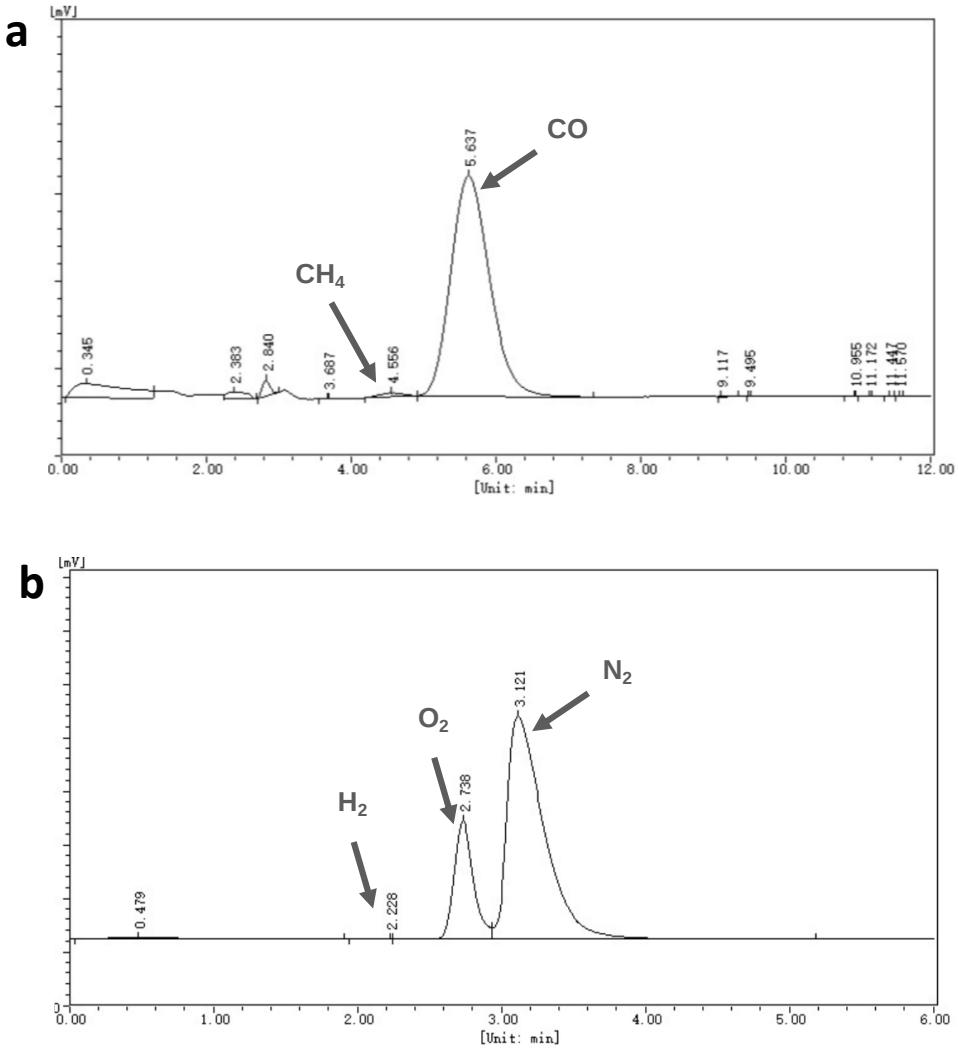

Fig. S15 The GC graph from (a) FID detector and (b) TCD detector.

The results highlight the negligible detection of other evolved gases, particularly CH_4 or H_2, ensuring high selectivity of BiOCl-NS towards CO.

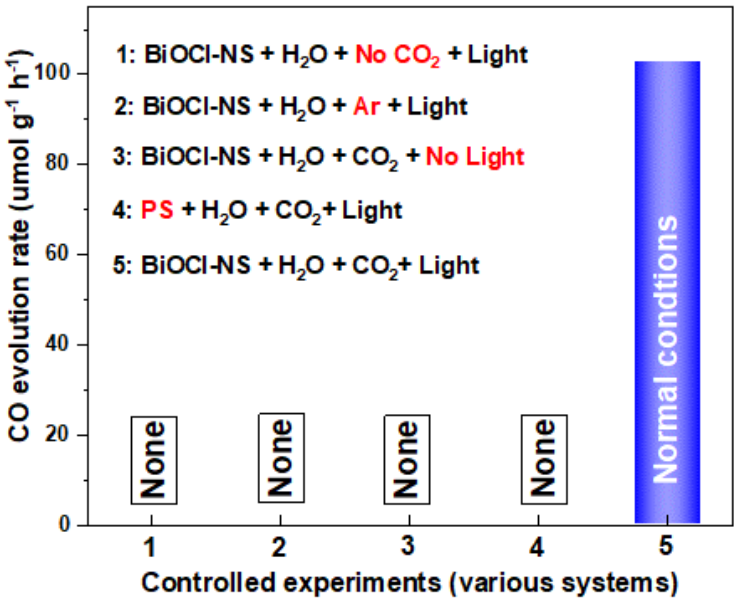

Fig. S16 The results of the control experiments under various conditions to verify the origin of the produced products.

Additional discussion:

Several control experiments were designed and conducted to determine the origin of evolved CO. For instance, system-1 was employed without feedstock CO_2, and in consequence, no CO was detected as a product, validating that feedstock CO_2 is necessary and is the origin of produced CO. This result also confirms that BiOCl-NS does not self-degrade during PCR. System 2, using argon (Ar) instead of CO_2, also fails to produce any CO, again highlighting that CO_2 is required to produce CO. Likewise, system 3 certifies the importance of light irradiation, as no CO was detected when the light was absent. Other than that, PS residues were not detected on the surface of BiOCl-NS, and hence unable to participate in PCR, to further endorse this, system-4 was processed, wherein PS was used as a photocatalyst instead of BiOCl-NS. The result confirms that no CO was produced, confirming that PS cannot participate during PCR. Finally, CO in high yield was detected when normal conditions were employed in system-5, namely, BiOCl-NS as photocatalysts, H_2O as a source of the proton, CO_2 as a feedstock, and light irradiation.

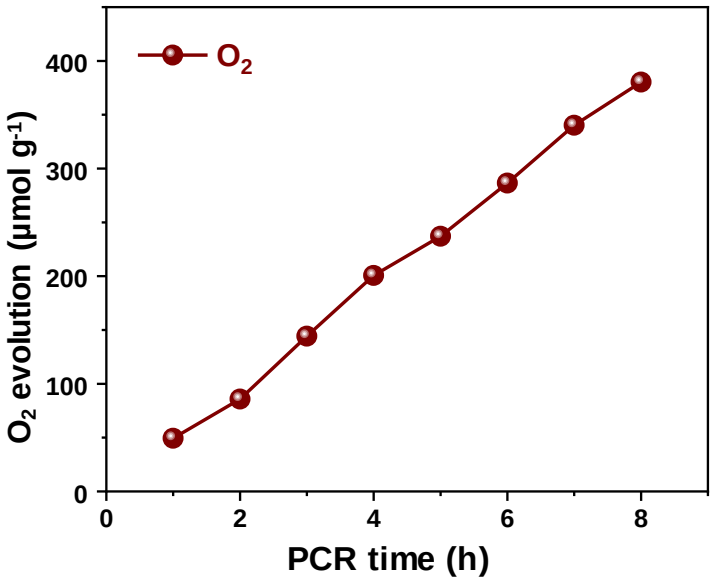

Fig. S17 The result shows the oxidation of water at the VB end of BiOCl-NS, due to which an uninterrupted supply of protons became available during PCR.

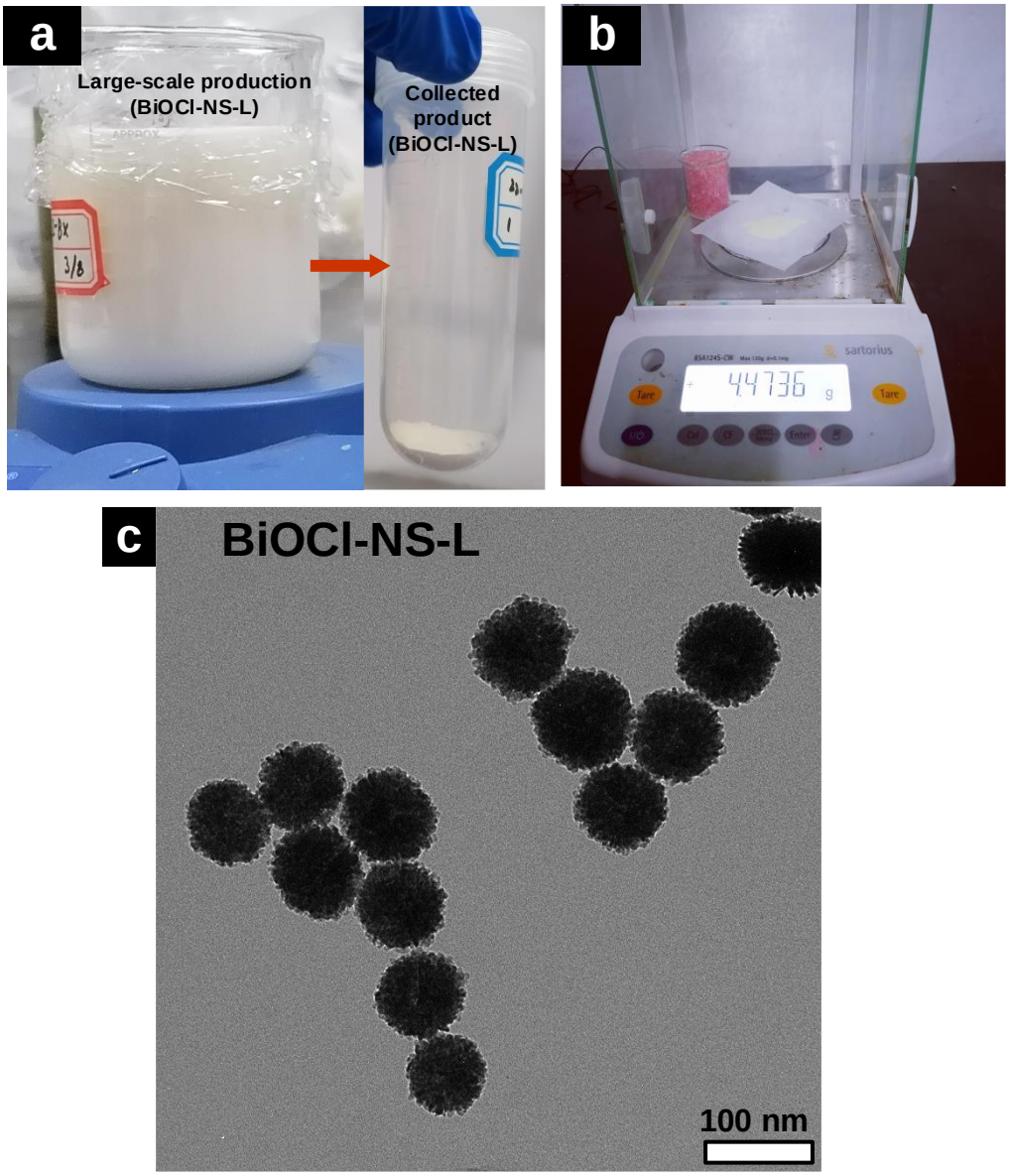

Fig. S18 (a) Large-scale synthesis of BiOCl nanospheres (named BiOCl-NS-L), and corresponding collected product. (b) gram-scale weightage, and (c) corresponding TEM image of BiOCl-NS-L displaying similar morphology as obtained in small-scale.

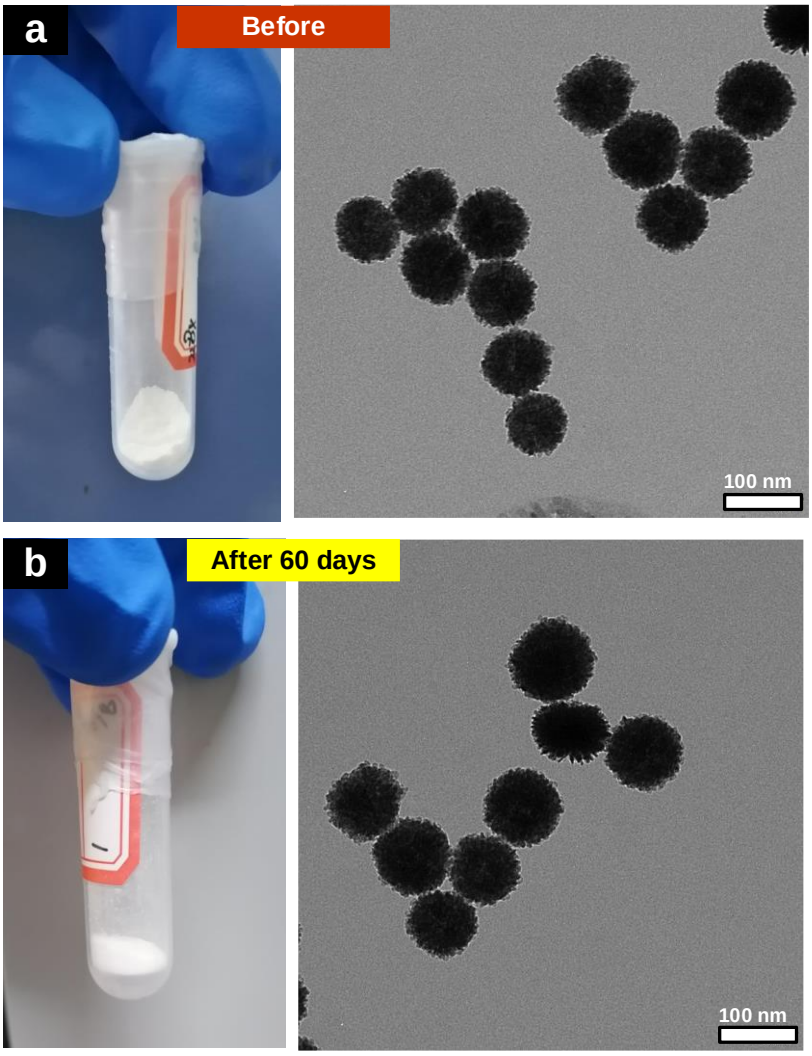

Fig. S19 Digital photograph and corresponding TEM images of BiOCl-NS (a) before and (b) after storing for months.

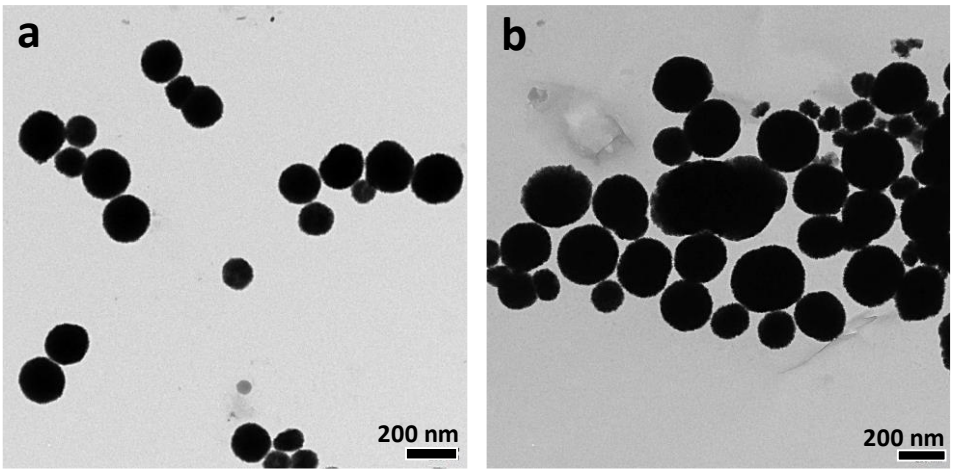

Fig. S20 TEM images of (a) BiOBr-NS, and (c) BiOI-NS, synthesized by changing the halogen precursors with NaBr and NaI, respectively.

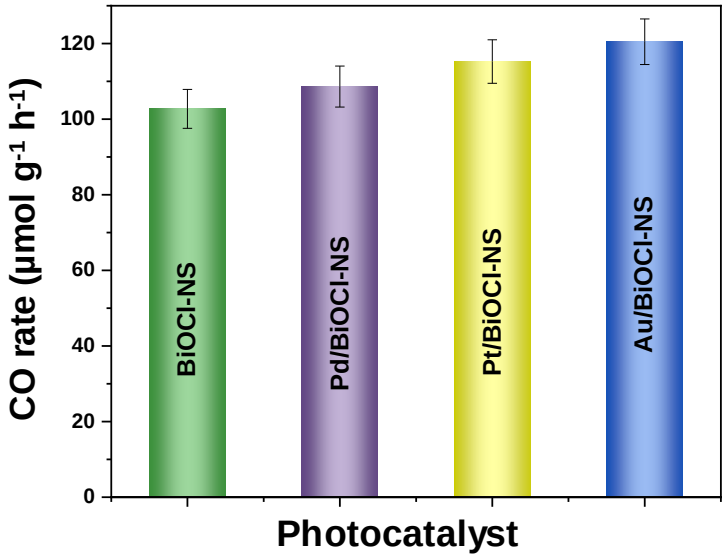

Fig. S21 The preliminary results highlight the further PCR optimization by introducing Nobel metals (Au, Pd, Pt) in BiOCl-NS, a valuable indicator for considering BiOCl-NS as a potential support material for diverse applications.

3. Supplementary Tables (S1-S4)

Table S1. Comparison of BiOCl-NS with 3D BiOX reported in the literature.

3D BiOX	Morphology	Synthesis	Approximate dia (nm)	Uniform/Non-uniform	Ref.
BiOCl	Flower-like	Solvothermal	~2 µm	Non-uniform	[1]
BiOCl	Mesopores flowers-like	Hydrothermal	>10 µm	Non-uniform	[2]
BiOCl	Flower-like	Solvothermal	~1 µm	Mildly-uniform	[3]
Bi-BiOCl	Flower-like	Mild-temperature	~2 µm	Non-uniform	[4]
H-BiOCl	Flower-like	Hydrothermal	~2 µm	Non-uniform	[5]
BiOCl	Flower-like	Solvothermal	~2 µm	Non-uniform	[6]
BiOCl/TiO_2	Hierarchical	Solvothermal	~2 µm	Non-uniform	[7]
BiOCl/CN	Aggregated sheet-like	Mild-Temperature	~3 µm	Non-uniform	[8]
P/Bi-BiOBr	Hierarchical	Solvothermal	~2 µm	Mildly-uniform	[9]
$BiVO_4$/BiOBr	Hierarchical	Solvothermal	~3 µm	Mildly-uniform	[10]
$BiOCl_xBr_{1-x}$	Hierarchical	colloidal	~3 µm	Non-uniform	[11]
BiOBr	Flower-like	hydrothermal	~2.5 µm	Non-uniform	[12]
BiOI	Hierarchical	Chemical-precipitation	~2.5 µm	Non-uniform	[13]
Pd/BiOI/MnOx	Hollow spheres	In-situ colloidal	>2 µm	Non-uniform	[14]
BiOBr/Bi_2SiO_5	Flower-like	Solvothermal	~2 µm	Non-uniform	[15]
BiOBr/$Cu_{2-x}S$	Flower-like	Solvothermal	~1.2 µm	Non-uniform	[16]
$BiOBr_{0.75}I_{0.25}$/$BiOIO_3$	Hierarchical	Solvothermal-assisted	>2 µm	Non-uniform	[17]
$BiOBr_xCl_{1-x}$	Buttercup-like	Colloidal	8-10 µm	Non-uniform	[18]
BiOI	Hierarchical	Solvothermal	1-3 µm	Non-uniform	[19]
$BiOCl_xBr_{1-x}$	Flower-like	Solvothermal	~1.5 µm	Non-uniform	[20]
$BiOCl_{0.6}Br_{0.4}$	Hierarchical	Solvothermal	~1.3 µm	Non-uniform	[21]
Bi_5O_7I	Porous Hierarchical	Solvothermal-calcination	~2 µm	Non-uniform	[22]
Anti-restack BiOCl	Hierarchitecture	Solvothermal	1–3µm	Non-uniform	[23]
BiOI	Flower-like	Precipitation	2–5 µm	Non-uniform	[24]
Bi-$BiOCl_x$	Hierarchical	Solvothermal	1–3µm	Non-uniform	[25]
BiOCl-NS	Self-organized spheres	Room-temperature	~76 nm	Uniform	This work

Table S2. The PCR over BiOCl-NS as compared with other recent state-of-the-art photocatalysts. The catalytic system does not involve any sensitizer, co-catalyst, scavengers, sacrificial agents, and organic solvents.

Photocatalyst	Catalyst dosage (mg)	Light source	CO evolving rate (μmol g^{-1} h^{-1})	CO_2 source	Ref.
$BiOIO_3$	20	300 W Xe (UV-vis)	17.33	H_2SO_4 + $NaHCO_3$	[26]
Br-grafted $Bi_2O_2(OH)(NO_3)$ NSs	20	300 W Xe (UV-vis)	8.12	H_2SO_4 + $NaHCO_3$	[27]
UN-$BiOIO_3$	50	300 W Xe (UV-vis)	5.42	H_2SO_4 + $NaHCO_3$	[28]
$Sr_2Bi_2Nb_2TiO_{12}$-OVs	10	300 W Xe (UV-vis)	11.7	H_2SO_4 + $NaHCO_3$	[29]
BiOBr	50	Xe (0.2 W cm^{-2})	4.45	H_2SO_4 + $NaHCO_3$	[30]
BiOI	50	300 W Xe (UV-vis)	5.18	H_2SO_4 + $NaHCO_3$	[31]
$Bi_{12}O_{17}Cl_2$ NTs	30	300 W Xe (UV-vis)	48.6	high-purity CO_2	[32]
BiOBr-OVs Atomic layers	10	300 W Xe (UV-vis)	87.4	high-purity CO_2	[33]
$BiOBr_xCl_{1-x}$	10	Xe (0.2 W cm^{-2})	15.86	high-purity CO_2	[18]
BiOCl	100	500 W Xe	1.01	high-purity CO_2	[34]
Co-Bi_3O_4Br atomic layer	30	300 W Xe (UV-vis)	107.1	high-purity CO_2	[35]
BiOCl with surface pits	10	300 W Xe (UV-vis)	89	high-purity CO_2	[36]
BiOCl-large surface area	10	300 W Xe (UV-vis)	11.42	high-purity CO_2	[36]
BiOCl-abundant OVs	10	300 W Xe (UV-vis)	23.45	high-purity CO_2	[36]
BiOCl- ultrathin thickness	10	300 W Xe (UV-vis)	14.33	high-purity CO_2	[36]
BiOCl-NS	10	300 W Xe (UV-vis)	102.72	high-purity CO_2	This work

Table S3. The PCR activity over BiOCl-NS in comparison with other recent state-of-the-art photocatalysts. The catalytic system is additive engaged e.g., it involves sensitizers, co-catalyst, scavengers, sacrificial agents, and organic solvents.

Photocatalyst	Light source	CO evolving ($\mu mol.g^{-1}h^{-1}$)	Co-Catalyst	Hole scavenger	Reaction medium	Ref.
g-C_3N_4	300 W Xe lamp (>400 nm)	17	Co-porphyrin	TEOA	CH_3CN	[37]
CdS	300 W Xe lamp (400 nm)	50.4	Co-ZIF-9	TEOA	$CH_3CN + H_2O$	[38]
MOF-525	300 W Xe lamp (400 nm)	200.6	Single-atom Co	TEOA	CH_3CN	[39]
o-PCN	300 W Xe lamp (>400 nm)	286	Pt	Na_2S+ Na_2SO_3	H_2O	[40]
UiO-66/C_3N_4	300 W Xe lamp (>400 nm)	59.4	-	TEOA	CH_3CN	[41]
Co-tuned Au nanoclusters	300 W Xe lam (420 nm)	3.451	-	TEOA	H_2O	[42]
Ni-doped CdS quantum dots	300 W Xe lamp (>400 nm)	9.5	dinuclear cobalt complex	TEOA	H_2O	[43]
$CsPbBr_3$/GO	100 W Xe lamp (150 mW cm−2)	23.7	-	-	Ethyl acetate	[44]
$CsPbBr_3$/g-C_3N_4	300 W Xe lamp (420 nm)	149	-	-	Acetonitrile/water and ethyl acetate/water	[45]
$Cs_2AgBiBr_6$	AM 1.5G, 150 mW cm−2	105	-	-	Ethyl acetate	[46]
BiOCl-NS	300 W Xe (UV-vis)	102.72			H_2O	This work

Table S4. The BiOCl-NS stability in PCR compared with some state-of-the-art photocatalysts.

Photocatalyst	Light source	Stability (h)	CO evolving (μmol g^{-1} h^{-1})	Reaction medium	Ref.
BiOCl@Bi_2O_3	>420 nm	36	30	H_2O	[47]
V_{Bi}-BiOBr NSs	UV-Vis	20	20.1	H_2O	[48]
Br-grafted	UV-Vis	12	8.12	H_2O (vapor)	[27]
$Bi_2O_2(OH)(NO_3)$ NSs $BiOIO_3$-OV	UV-Vis	12	17.33	H_2O (vapor)	[26]
$Sr_2Bi_2Nb_2TiO_{12}$-OV	UV-Vis	4	17.11	H_2O (vapor)	[29]
$Bi_4Ti_3O_{12}$-UOV	UV-Vis	4	11.7	H_2O (vapor)	[49]
BiOBr-Ovs Atomic Layers	>420 nm	60	87.4	H_2O	[33]
$Bi_{12}O_{17}Cl_2$ NTs	UV-Vis	12	48.6	H_2O	[32]
Partially oxidized SnS_2 atomic layers	>420 nm	12.28	20	H_2O (vapor)	[50]
BP@g-C_3N_4	UV-Vis	8	6.54	H_2O (vapor)	[51]
SiC-NW/C	UV-Vis	9	5.87	H_2O (vapor)	[52]
Ni-SA-5/ZrO_2	UV-Vis	25	11.8	H_2O (vapor)	[53]
BiOCl-NS	UV-Vis	32	102.72	H_2O	This work

Table S5. The AQE of BiOCl-NS in PCR compared with some state-of-the-art BiOX photocatalysts.

Photocatalyst	AQE (%)	References
S-BiOCl	0.28	[54]
C_3N_4/bismuthene/BiOCl	0.42	[55]
BiOBr-5	0.33	[56]
$Bi_4O_5Br_xI_{2-x}$	0.37	[57]
Bi_4O_5I−Fe30	0.12	[58]
Pt_1/BOB-V_O	0.20	[59]
$BiOIO_3$-b_3	0.10	[28]
BiOCl-NS	0.51	This work

4. Supplementary References

1 S. Zhao, Y. Zhang, Y. Zhou, C. Zhang, X. Sheng, J. Fang and M. Zhang, *ACS Sustain. Chem. Eng.*, 2017, **5**, 1416-1424.

2 W. Li, Y. Mao, Z. Liu, J. Zhang, J. Luo, L. Zhang and Z. A. Qiao, *Adv. Mater.*, 2023, **35**, 2300396.

3 C. Huang, J. Hu, S. Cong, Z. Zhao and X. Qiu, *Appl. Catal. B*, 2015, **174-175**, 105-112.

4 S. Gong, G. Zhu, R. Wang, F. Rao, X. Shi, J. Gao, Y. Huang, C. He and M. Hojamberdiev, *Appl. Catal. B*, 2021, **297**, 120413.

5 Q. Li, J. Ren, Y.-j. Hao, Y.-l. Li, X.-j. Wang, Y. Liu, R. Su and F.-t. Li, *Appl. Catal. B*, 2022, **317**, 121761.

6 X. Ren, M. Gao, Y. Zhang, Z. Zhang, X. Cao, B. Wang and X. Wang, *Appl. Catal. B*, 2020, **274**, 119063.

7 W. Li, Y. Tian, H. Li, C. Zhao, B. Zhang, H. Zhang, W. Geng and Q. Zhang, *Appl. Catal. A*, 2016, **516**, 81-89.

8 X. Hu, Y. Zhang, B. Wang, H. Li and W. Dong, *Appl. Catal. B*, 2019, **256**, 117789.

9 J.-y. Zhu, Y.-p. Li, X.-j. Wang, J. Zhao, Y.-s. Wu and F.-t. Li, *ACS Sustain. Chem. Eng.*, 2019, **7**, 14953−14961.

10 H. Razavi-Khosroshahi, S. Mohammadzadeh, M. Hojamberdiev, S. Kitano, M. Yamauchi and M. Fuji, *Adv. Powder Technol.*, 2019, **30**, 1290-1296.

11 H. Gnayem and Y. Sasson, *ACS Catal.*, 2013, **3**, 186-191.

12 W. Qingli, M. Zerui, Z. Yanfeng, Y. Tingjiang, M. Lingpeng and W. Xuxu, *ACS Catal.*, 2022, **12**, 4016-4025.

13 H. Huang, K. Xiao, X. Du and Y. Zhang, *ACS Sustain. Chem. Eng.*, 2017, **5**, 5253-5264.

14 Y. Huang, H. Xu, H. Yang, Y. Lin, H. Liu and Y. Tong, *ACS Sustain. Chem. Eng.*, 2018, **6**, 2751−2757.

15 J. Wang, G. Zhang, J. Li and K. Wang, *ACS Sustain. Chem. Eng.*, 2018, **6**, 14221-14229.

16 X. Li, Q. Liu, F. Deng, J. Huang, L. Han, C. He, Z. Chen, Y. Luo and Y. Zhu, *Appl. Catal. B*, 2022, **314**, 121502.

17 C. Zeng, Y. Hu and H. Huang, *ACS Sustain. Chem. Eng.*, 2017, **5**, 3897-3905.

18 M. Gao, J. Yang, T. Sun, Z. Zhang, D. Zhang, H. Huang, H. Lin, Y. Fang and X. Wang, *Appl. Catal. B*, 2019, **243**, 734-740.

19 G. Dong, W. Ho and L. Zhang, *Appl. Catal. B*, 2015, **168-169**, 490–496.

20 W. Huo, W. Xu, Z. Guo, Y. Zhang and F. Dong, *Appl. Catal. B*, 2020, **284**, 119694.

21 W. J. Kim, D. Pradhan, B.-K. Min and Y. Sohn, *Appl. Catal. B*, 2014, **147**, 711-725.

22 Y. Liu, G. Zhu, J. Gao, R. Zhu, M. Hojamberdiev, C. Wang, X. Wei and P. Liu, *Appl. Catal. B*, 2017, **205**, 421-432.

23 Y. Mi, L. Wen, Z. Wang, D. Cao, Y. Fang and Y. Lei, *Appl. Catal. B*, 2015, **176-177**, 331-337.

24 M. Sun, Q. Wei, Y. Shao, B. Du, T. Yan, L. Yan and D. Li, *Appl. Catal. B*, 2018, **233**, 250-259.

25 H. Wang, W. Zhang, X. Li, J. Li, W. Cen, Q. Li and F. Dong, *Appl. Catal. B*, 2018, **225**, 218-227.

26 F. Chen, Z. Ma, L. Ye, T. Ma, T. Zhang, Y. Zhang and H. Huang, *Adv. Mater.*, 2020, **32**, 1908350.

27 L. Hao, L. Kang, H. Huang, L. Ye, K. Han, S. Yang, H. Yu, M. Batmunkh, Y. Zhang and T. Ma, *Adv. Mater.*, 2019, **31**, 1900546.

28 F. Chen, H. Huang, L. Ye, T. Zhang, Y. Zhang, X. Han and T. Ma, *Adv. Funct. Mater.*, 2018, **28**, 1804284.

29 H. Yu, J. Li, Y. Zhang, S. Yang, K. Han, F. Dong, T. Ma and H. Huang, *Angew. Chem. Int. Ed.*, 2019, **58**, 3880-3884.

30 D. Wu, L. Ye, H. Y. Yip and P. K. Wong, *Catal. Sci. Technol.*, 2017, **7**, 265-271.

31 L. Ye, X. Jin, X. Ji, C. Liu, Y. Su, H. Xie and C. Liu, *Chem. Eng. J.*, 2016, **291**, 39-46.

32 J. Di, C. Zhu, M. Ji, M. Duan, R. Long, C. Yan, K. Gu, J. Xiong, Y. She, J. Xia, H. Li and Z. Liu, *Angew. Chem. Int. Ed.*, 2018, **57**, 14847-14851.

33 J. Wu, X. Li, W. Shi, P. Ling, Y. Sun, X. Jiao, S. Gao, L. Liang, J. Xu, W. Yan, C. Wang and Y. Xie, *Angew. Chem. Int. Ed.*, 2018, **57**, 8719-8723.

34 L. Zhang, W. Wang, D. Jiang, E. Gao and S. Sun, *Nano Res.*, 2014, **8**, 821–831.

35 J. Di, C. Chen, S. Z. Yang, S. Chen, M. Duan, J. Xiong, C. Zhu, R. Long, W. Hao, Z. Chi, H. Chen, Y. X. Weng, J. Xia, L. Song, S. Li, H. Li and Z. Liu, *Nat. Commun.*, 2019, **10**, 2840.

36 M. Z. Shahid, Z. Chen, R. Mehmood, S. Zheng, A. M. Idris and Z. Li, *Mater. Today Energy*, 2023, **34**, 101303.

37 G. Zhao, H. Pang, G. Liu, P. Li, H. Liu, H. Zhang, L. Shi and J. Ye, *Appl. Catal. B*, 2017, **200**, 141-149.

38 S. Wang and X. Wang, *Appl. Catal. B*, 2015, **162**, 494-500.

39 H. Zhang, J. Wei, J. Dong, G. Liu, L. Shi, P. An, G. Zhao, J. Kong, X. Wang, X. Meng, J. Zhang and J. Ye, *Angew. Chem. Int. Ed.*, 2016, **55**, 14310-14314.

40 A. Li, Q. Cao, G. Zhou, B. Schmidt, W. Zhu, X. Yuan, H. Huo, J. Gong and M. Antonietti, *Angew. Chem. Int. Ed.*, 2019, **58**, 14549-14555.

41 L. Shi, T. Wang, H. Zhang, K. Chang and J. Ye, *Adv. Funct. Mater.*, 2015, **25**, 5360-5367.

42 X. Cui, J. Wang, B. Liu, S. Ling, R. Long and Y. Xiong, *J. Am. Chem. Soc.*, 2018, **140**, 16514-16520.

43 J. Wang, T. Xia, L. Wang, X. Zheng, Z. Qi, C. Gao, J. Zhu, Z. Li, H. Xu and Y. Xiong, *Angew. Chem. Int. Ed.*, 2018, **57**, 16447-16451.

44 Y. F. Xu, M. Z. Yang, B. X. Chen, X. D. Wang, H. Y. Chen, D. B. Kuang and C. Y. Su, *J. Am. Chem. Soc.*, 2017, **139**, 5660-5663.

45 M. Ou, W. Tu, S. Yin, W. Xing, S. Wu, H. Wang, S. Wan, Q. Zhong and R. Xu, *Angew. Chem. Int. Ed.*, 2018, **57**, 13570-13574.

46 L. Zhou, Y. F. Xu, B. X. Chen, D. B. Kuang and C. Y. Su, *Small*, 2018, **14**, 1703762.

47 L. Wang, X. Zhao, D. Lv, C. Liu, W. Lai, C. Sun, Z. Su, X. Xu, W. Hao, S. X. Dou and Y. Du, *Adv. Mater.*, 2020, **32**, 2004311.

48 J. Di, C. Chen, C. Zhu, P. Song, J. Xiong, M. Ji, J. Zhou, Q. Fu, M. Xu, W. Hao, J. Xia, S. Li, H. Li and Z. Liu, *ACS Appl. Mater. Interfaces*, 2019, **11**, 30786−30792.

49 L. Liu, H. Huang, F. Chen, H. Yu, N. Tian, Y. Zhang and T. Zhang, *Sci. Bull.*, 2020, **65**, 934-943.

50 X. Jiao, X. Li, X. Jin, Y. Sun, J. Xu, L. Liang, H. Ju, J. Zhu, Y. Pan, W. Yan, Y. Lin and Y. Xie, *J. Am. Chem. Soc.*, 2017, **139**, 18044-18051.

51 C. Han, J. Li, Z. Ma, H. Xie, G. I. N. Waterhouse, L. Ye and T. Zhang, *Sci. China Mater.*, 2018, **61**, 1159-1166.

52 W. Weng, S. Wang, W. Xiao and X. W. D. Lou, *Adv. Mater.*, 2020, **32**, 2001560.

53 X. Xiong, C. Mao, Z. Yang, Q. Zhang, G. I. N. Waterhouse, L. Gu and T. Zhang, *Adv. Energy Mater.*, 2020, **10**, 2002928.

54 K. Yan, L. Chen, Y. Hu, T. Wang, C. Chen, C. Gao, Y. Huang and B. Li, *Nano Res.*, 2023, DOI: 10.1007/s12274-023-5888-3.

55 D. Zhang, X. Cui, L. Liu, Y. Xu, J. Zhao, J. Han and W. Zheng, *ACS Appl. Mater. Interfaces*, 2021, **13**, 21582−21592.

56 J. Meng, Y. Duan, S. Jing, J. Ma, K. Wang, K. Zhou, C. Ban, Y. Wang, B. Hu, D. Yu, L. Gan and X. Zhou, *Nano Energy*, 2022, **92**, 106671.

57 Y. Bai, L. Ye, T. Chen, P. Wang, L. Wang, X. Shi and P. K. Wong, *Appl. Catal. B*, 2017, **203**, 633-640.

58 X. Jin, C. Lv, X. Zhou, H. Xie, S. Sun, Y. Liu, Q. Meng and G. Chen, *Nano Energy*, 2019, **64**, 103955.

59 G. Ren, M. Shi, Z. Li, Z. Zhang and X. Meng, *Appl. Catal. B*, 2023, **327**, 122462.